5728 *Macromolecules* **2009**, *42*, 5728–5740
DOI: 10.1021/ma802479c

Macromolecules
ARTICLE

Saturation of Pointlike Nuclei and the Transition to Oriented Structures in Flow-Induced Crystallization of Isotactic Polypropylene

Jan-Willem Housmans,[†,‡] Rudi J. A. Steenbakkers,[†] Peter C. Roozemond,[†] Gerrit W. M. Peters,*[,†] and Han E. H. Meijer[†]

[†]*Department of Mechanical Engineering, Eindhoven University of Technology, P.O. Box 513, 5600 MB Eindhoven, The Netherlands, and* [‡]*The Dutch Polymer Institute (DPI), PO Box 902, 5600 AX, Eindhoven, The Netherlands*

Received November 5, 2008; Revised Manuscript Received June 4, 2009

ABSTRACT: The influence of molecular weight and processing conditions on the crystallization kinetics of isotactic polypropylene is studied using rheometry. Flow-induced crystallization experiments are performed with shear rates at which molecular stretch of the longest chains is expected. Depending on the molecular weight, a saturation of pointlike nuclei is observed with increasing shear time. In most cases, the process accelerates after sufficient flow time, and this change in kinetics is due to the occurrence of fibrillar nucleation resulting in the formation of row structures and/or shishes. The number of pointlike nuclei is derived from the rheometry experiments by modeling the system as a suspension. This method has some important advantages, i.e., (1) it is applicable to systems where optical microscopy does not work (i.e., colored systems) and (2) it is much easier, faster, and more accurate than optical methods.

1. Introduction

The properties of semicrystalline polymer products strongly depend on the final morphology, which itself depends on both the molecular properties of the polymer used and the conditions during production processes like injection molding, film blowing, and/or fiber spinning. These conditions are often extreme; the material is subjected to high pressures, high deformation rates, and high cooling rates. Moreover, the flow history can have a complex nature; i.e., the material experiences mixed deformation modes. To separate the influence of flow and temperature on the crystallization behavior, the short-term shearing protocol, introduced by Janeschitz-Kriegl and co-workers,[1] has been applied by several researchers using either commercial equipment like rheometers,[2−5] the Linkam shear cell,[5−7] or in-house developed setups.[1,8−12] It was shown that by applying flow the crystallization process is accelerated, more specific the nucleation process, resulting in a change in morphology. The importance of the high molecular weight (HMW) tail on the formation of oriented, anisotropic structures was pointed out.[2,13−15] The effect is ascribed to the entanglements between the long chains, since for strong enough flows these chains are extended between these constraints.

A rheological classification of different flow regimes, derived from molecular based rheology and rubber elasticity theory, was proposed by van Meerveld et al.[16] The transitions between the different flow regimes, and the associated physical processes governing the flow-induced crystallization (FIC) process, are characterized by critical values of the Deborah (*De*) or Weissenberg (*Wi*)[50] numbers related to molecular orientation and to molecular stretch of the HMW tail. An extensive evaluation of experimental results from the literature illustrates that the transition from an enhanced point nucleation rate toward the development of fibrillar structures correlates with the transition from chain segment orientation to chain stretch of the high molecular weight chains in the melt. Although the classification gives an indication in which flow regime experiments are performed, and whether fibrillar morphologies will develop or not, flow time is not specifically included. It is stated that the flow time, t_s, has to be sufficiently long in order to fulfill the condition $\lambda > \lambda^*(T)$; i.e., the molecular stretch ratio λ has to be larger than a certain critical, temperature-dependent value $\lambda^*(T)$, marking the transition between weak and strong stretching conditions. However, we expect that this critical value has to be maintained long enough to cause significant shish growth.

As was shown by many researchers, the combination of flow strength and flow time (t_s) influences the rate of crystallization in a complex way. The simplest measure one could think of to capture these effects is the total applied shear strain defined as $\gamma = \dot{\gamma} t_s$. However, the shear rate, $\dot{\gamma}$, has a more pronounced influence than t_s, i.e., a shear flow at a high $\dot{\gamma}$ for a short time accelerates the process more than a shear flow at a low $\dot{\gamma}$ for longer times.[2] For short-term shear experiments, i.e., experiments for which the shear time is short compared to the time scale of the subsequent crystallization process, applying constant shear stress, Liedauer et al.[1] and Eder and Janeschitz-Kriegl[18] found an empirical relationship for the number of flow-induced point nuclei, $N \sim \dot{\gamma}^2 t_s$, and it was observed that the transition from spherulitic to fibrillar morphology was marked by $\dot{\gamma}^4 t_s$. These relations can be thought of as scaling laws that relate the flow time to the structures obtained and could lead to the derivation of a critical value for the duration of flow. In a later paper, Janeschitz-Kriegl et al.[19] presented the concept that the governing variable for FIC is the mechanical work applied (eq 1). Moreover, according to them there is a sudden transition from pointlike to oriented nuclei (shish) when the work applied is large enough; i.e., as soon as the number of nuclei becomes sufficiently large, they aggregate forming shishes. The work measure used, was defined as

$$w = \bar{\eta} \int_0^{t_s} \dot{\gamma}^2(t)\, \mathrm{d}t \qquad (1)$$

*To whom correspondence should be addressed.

 Published on Web 07/07/2009

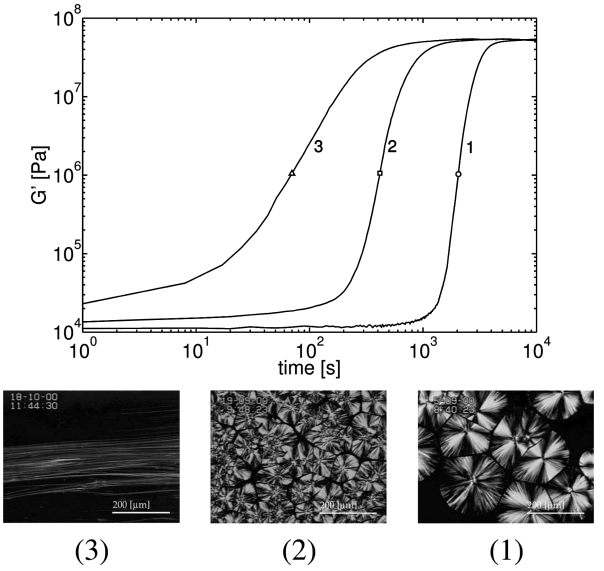

Figure 1. Evolution of the storage modulus during crystallization of iPP HD120MO at $T_{exp} = 135$ °C, measured under quiescent conditions (○, 1) and after shearing at $\dot{\gamma} = 60\ s^{-1}$ for $t_s = 1$ s (□, 2) and $t_s = 6$ s (Δ, 3). Optical micrographs indicate the characteristic morphology for the three crystallization experiments.[28]

where $\bar{\eta}$ is the viscosity, averaged over the shear rates experienced, and $\dot{\gamma}$ the time-dependent shear rate. Slopes of log(N) vs log(w) lay between 2 and 4, increasing with increasing temperature, which is a different behavior than the previously formulated criterium by Liedauer et al.[1] Recently, the concept of a critical work was also used by the group of Ryan in Sheffield for the analysis of FIC of model linear−linear blends of hydrogenated polybutadiene (h-PBD) in a rotational shear device. They found that a critical amount of work is required for shish formation, which depends on the molecular weight distribution (MWD) of the polymer and becomes independent of the shear rate as soon as it exceeds the inverse of the longest Rouse time,[20] which is in line with the classification of van Meerveld et al.[16]

The relations between flow conditions and resulting morphology presented above are based on the kinematics of the flow and not on the dynamics of molecules experiencing these kinematics, as proposed by Zuidema et al.[21] In their numerical work on modeling of flow-induced crystallization, they used the recoverable strain, a direct measure for the stored elastic energy and thus for the molecular orientation and stretch, as the driving force for the formation of threadlike precursors. This choice was made following the conclusion from McHugh et al.[22] that molecular strain is the controlling process parameter.

In this paper the crystallization process of isotactic polypropylene (iPP) is studied using rotational rheometry. This widely used experimental technique combines the possibility to apply flow and, subsequently, mechanical spectrometry to detect even small changes in the material, e.g., due to the onset of crystallization. Therefore, rheometry is a good candidate to become a standard method in polymer processing for FIC characterization. For three iPP grades sheared at different shear rates, the influence of flow time on the change in nucleation density and the formation of fibrillar structures is investigated. The observed change in kinetics, which is related to the formation of oriented structures, is correlated to the critical work concept. Furthermore, existing knowledge on FIC is applied to derive morphological information from the results. The evolution of space filling (ϕ) is based on modeling the crystallizing polymer as a suspension of (semicrystalline) particles in an (amorphous) matrix.[23] The number of nuclei is estimated from space filling using the Avrami

Table 1. Physical Properties of the Three iPP Grades: M_w, M_w/M_n, T_m, X_c, and T_c

name	grade	M_w [kg/mol]	M_w/M_n	T_m [°C]	X_c [%]	T_c [°C]
iPP1	HD234CF	310	3.4	159	48	110
iPP2	HD120MO	365	5.4	163	47	113
iPP3	13E10	636	6.9	162	47	117

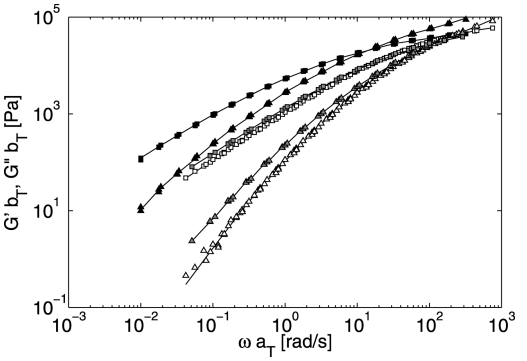

Figure 2. Storage (Δ) and loss (□) modulus at $T_{ref} = 220$ °C. iPP1: open symbols; iPP2: gray symbols; iPP3: black symbols.

equation, a method already successfully applied to obtain nuclei density from isothermal DSC experiments.[24] Where DSC provides only the number of nuclei under quiescent conditions, rheometry allows to include the influence of flow, provided that the procedure followed indeed works. The important advantages of the method are (1) it is applicable to systems where optical microscopy does not work (i.e., colored systems) and (2) it is much easier, faster, and more accurate than optical methods.

2. Experimental Section

2.1. Materials. Three isotactic polypropylene homopolymer grades (iPP) with different molecular weight distributions are used. The low molecular weight grade, Borealis HD234CF, has a weight-average molecular weight $M_w \approx 310$ kg/mol and a polydispersity $M_w/M_n \approx 3.4$.[25] The second grade, Borealis HD120MO, has a slightly higher molecular weight ($M_w = 365$ kg/mol) and a broader MW distribution ($M_w/M_n = 5.4$).[26,27] The high molecular weight grade, DSM 13E10, has an M_w of 636 kg/mol and a M_w/M_n of 6.9 and has been used in several crystallization studies.[2,26,28] For convenience, the three grades are labeled iPP1, iPP2, and iPP3, respectively.

2.2. Differential Scanning Calorimetry (DSC). The melting temperature (T_m), melting enthalpy (ΔH_m), and crystallization temperature (T_c) are determined using a Mettler Toledo DSC (DSC823e) and a heating and cooling rate of 10 °C min^{-1} on samples with a weight of 3 ± 0.5 mg. A second heating cycle is performed to have a homogeneous sample distribution in the pan from which T_m and ΔH_m are obtained. Crystallinity is determined using $X_c = \Delta H_m/\Delta H_{m0}$ with the melting enthalpy for a 100% crystalline material, $\Delta H_{m0} = 209$ J/g.[29]

2.3. Rheological Properties in the Melt State. A Rheometrics ARES rheometer is used with a plate−plate geometry, diameter of the plates of 25 mm, for small-amplitude oscillatory shear measurements. The characteristic rheological properties (storage and loss modulus, G' and G'', and loss angle, δ) are obtained over a broad range of temperatures (from 145 to 250 °C) and angular frequencies, ω (from 0.01 to 100 rad s^{-1}). The lower limit of ω for the lowest temperature is 0.1 rad s^{-1} to avoid changes due to crystallization. To determine the rheological properties in the linear viscoelastic regime, the strain applied is determined from strain sweeps and set to 5% for all measurements. The experiments are performed in a nitrogen environment to avoid degradation of the material. Time−temperature superposition is applied to obtain mastercurves at a reference temperature of 220 °C.

Table 2. Rheological Parameters at 220 °C for the Materials Studied: Time−Temperature Shift Factors, a_T and b_T, Arrhenius Activation Energy, E_a, and Maxwell Relaxation Spectra, g_i and τ_i

iPP1	T [°C]	a_T	b_T	T_{ref} [°C]		E_a [kJ/mol]
	145	7.500 16	0.886 49	220		43.0
	160	4.547 93	0.931 54	mode	$g_i \times 10^{-4}$ [Pa]	τ_i [s]
	175	2.915 01	0.953 63	1	11.08	0.0011
	190	2.111 67	0.971 34	2	3.38	0.0085
	205	1.425 67	1.004 86	3	0.870	0.0448
	220	1	1	4	0.106	0.237
	235	0.747 55	1.059 51	5	0.004	1.46
	250	0.665 50	1.233 71			
iPP2	T [°C]	a_T	b_T	T_{ref} [°C]		E_a [kJ/mol]
	160	2.879 37	1.106 02	220		32.6
	190	1.619 19	0.910 01	mode	$g_i \times 10^{-4}$ [Pa]	τ_i [s]
	220	1	1	1	9.34	0.0014
	250	0.601 71	1.120 35	2	2.76	0.0114
				3	0.769	0.0591
				4	0.130	0.298
				5	0.011	1.67
				6	0.0004	11.5
iPP3	T [°C]	a_T	b_T	T_{ref} [°C]		E_a [kJ/mol]
	160	3.424 41	0.878 36	220		40.3
	190	1.925 69	0.939 18	mode	$g_i \times 10^{-4}$ [Pa]	τ_i [s]
	220	1	1	1	9.86	0.0007
	250	0.555 53	1.060 82	2	5.62	0.0044
				3	3.40	0.0227
				4	1.61	0.109
				5	0.53	0.521
				6	0.121	2.502
				7	0.019	13.4
				8	0.0017	97.3

2.4. Flow-Induced Crystallization Experiments. Crystallization kinetics is followed using rheology. A plate−plate geometry of 8 mm is used to avoid transducer instabilities. The experimental procedure is as follows:

- Samples are molten at a temperature of 230 °C for 10 min to remove any history before the start of the test.
- Subsequently, the samples are cooled to the desired temperature (T_{exp} = 138 °C) at which the isothermal crystallization experiments are performed, with a controlled cooling rate of 15 °C min^{-1} to avoid any undershoot. The gap is adjusted continuously to compensate for thermal expansion (shrinkage) of the samples.
- Oscillatory tests using an angular frequency of 5 rad s^{-1} and a strain of 0.5% are performed to monitor the evolution of G', G'', and δ in time.

For short-term FIC experiments, a shear flow with a varying shear rate, $\dot{\gamma}$, for different shear times, t_s, is applied prior to the third step. The choice of $\dot{\gamma}$ is determined from the rheological characterization of the three materials and is set to be higher than the critical value that determines the transition from the orientation to the stretch regime, i.e., the inverse of the longest stretch or Rouse time.

3. Theoretical Considerations

Figure 1 shows flow-induced crystallization experiments on iPP2 (Vega, J. F., personal communication, used in ref 23) that follow the above-mentioned procedure (T_{exp} = 135 °C). The figure is illustrative for the results expected. The storage modulus, $G'(\phi)$, evolves with the growing crystallites in the melt, since it is a function of degree of space filling, ϕ. When flow is applied, the two main observations are: (1) Curve 2: an acceleration of the crystallization process, the modulus curve shifts to lower times. The shape is similar to that of the quiescent experiment. (2) Curve 3: for longer flow times, the modulus curve shifts to lower times, but now its shape changes (the slope decreases). The kinetics of

Table 3. Longest Reptation Time (τ_{rep}^{HMW}) Determined from the Maxwell Spectrum and Stretch Time Corresponding to the Highest Mode, τ_s^{HMW}, at T = 138 °C

	iPP1		iPP2		iPP3	
	τ_{rep}^{HMW}	τ_s^{HMW}	τ_{rep}^{HMW}	τ_s^{HMW}	τ_{rep}^{HMW}	τ_s^{HMW}
relaxation times [s]	11.8	0.066	56.3	0.27	690	1.9
$\dot{\gamma}_{I\to II}$ [s^{-1}][a]	0.085		0.02		0.001	
$\dot{\gamma}_{II\to III}$ [s^{-1}][a]		15		3.7		0.53

[a] $\dot{\gamma}_{I\to II}$ and $\dot{\gamma}_{II\to III}$ are critical values of the shear rate for the transition between regime I and II and regime II and III, respectively.

degree of space filling is usually described by the Avrami equation:[30,31]

$$\phi = 1-\exp[-Ct^n] \tag{2}$$

where C is the overall rate of crystallization and n the Avrami exponent, which reflects the crystal dimensionality and the type of nucleation (heterogeneous, i.e., predetermined, or sporadic).[24] When nucleation is heterogeneous and the crystal growth rate, G, is constant, the n values of 1, 2, and 3 correspond to a crystal geometry of rods (1-dimensional, 1D), disks (2-dimensional, 2D), and spheres (3-dimensional, 3D), respectively. For sporadic nucleation at a constant rate, the n values of 2, 3, and 4 correspond to the crystal geometry of rods, disks, and spheres.[31,32] For the change of the modulus, it can be derived that

$$\frac{dG'}{dt} = \frac{dG'}{d\phi}\frac{d\phi}{dt} \tag{3}$$

in which $d\phi/dt$ is given by (using eq 2)

$$\frac{d\phi}{dt} = Cnt^{n-1}(1-\phi) \tag{4}$$

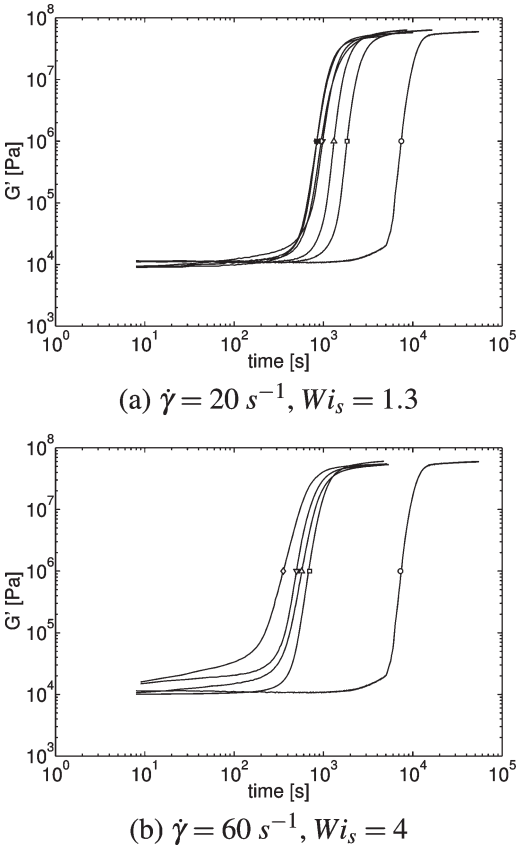

Figure 3. Time buildup of the storage modulus for iPP1 at T_c = 138 °C under quiescent conditions (○) and after flow application: (a) ($\dot{\gamma}$ = 20 s^{-1}, Wi_s = 1.3) for 1 s (□), 2 s (Δ), 6 s (▽), 8 s (◊), 10 s (∗), and 12 s (■); (b) ($\dot{\gamma}$ = 60 s^{-1}, Wi_s = 4) for 1 s (□), 2 s (Δ), 3 s (▽), and 4 s (◊).

If two double-logarithmic modulus vs time curves, labeled a and b, have the same shape but are shifted relative to each other along the time axis, then

$$t_a \left.\frac{dG'_a}{dt}\right|_{t=t_a} = t_b \left.\frac{dG'_b}{dt}\right|_{t=t_b} \quad (5)$$

for any two points on a and b with the same modulus, $G'_a(t_a) = G'_b(t_b)$. Combining this with eqs 3 and 4 gives

$$\left.\frac{dG'_a}{d\phi}\right|_{\phi=\phi_a} C_a n_a t_a^{n_a}(1-\phi_a) = \left.\frac{dG'_b}{d\phi}\right|_{\phi=\phi_b} C_b n_b t_b^{n_b}(1-\phi_b) \quad (6)$$

Considering that G' is a unique (as yet unspecified) function of ϕ, so that $\phi_a(t_a) = \phi_b(t_b)$ and, from eq 2, $C_a t_a^{n_a} = C_b t_b^{n_b}$, we get

$$n_a = n_b \quad (7)$$

This means that, to achieve a shift along the time axis, only C changes. We assume that the growth rate is only a function of temperature. Therefore, the shift indicates an increase in the number of nuclei. A change in slope corresponds to a change in n, i.e., the dimensionality of the growth process. Under quiescent conditions in the temperature range applied, no sporadic nucleation occurs, and the number of nuclei, N, is constant. Crystal lamellae grow with a constant growth rate, G, in all directions, thus a 3D growth, from these nuclei forming spherulites (Figure 1, micrograph 1[28]). In that case, $n = 3$ and $C = (4/3)\pi NG^3$.[5,18,24,31] Flow, applied for a short time, only leads to a shift in modulus (curve 2). This implies that the same type of morphology is formed as in the quiescent case (spherulites), but with a higher number density, N, since C increases and the growth rate G is

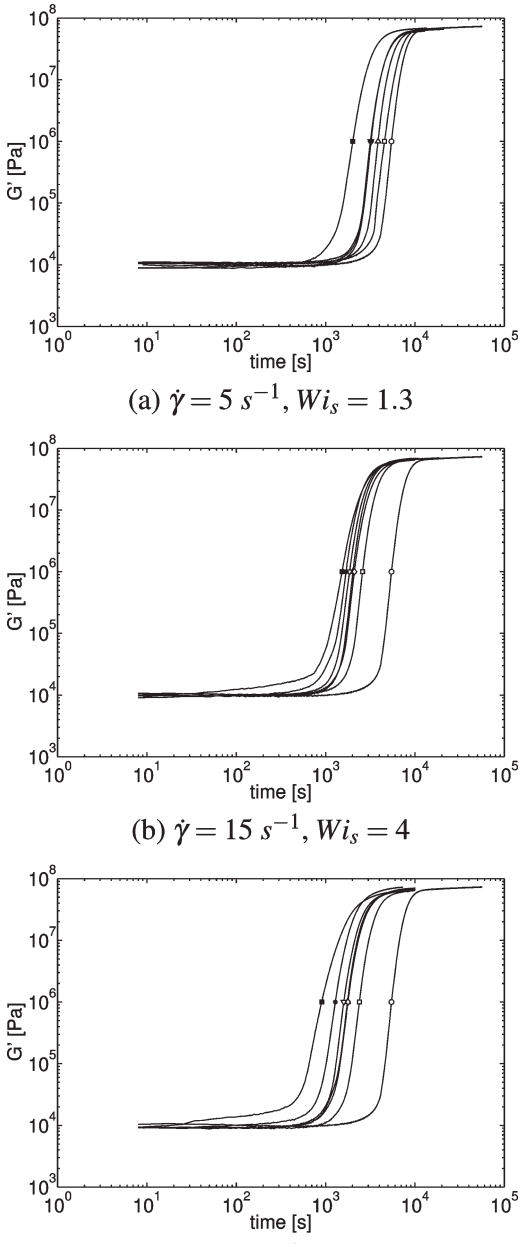

Figure 4. Time buildup of the storage modulus for iPP2 at T_c = 138 °C under quiescent conditions (○) and after flow application: (a) ($\dot{\gamma}$ = 5 s^{-1}, Wi_s = 1.3) for 2 s (□), 5 s (Δ), 10 s (▽), 20 s (◊), 40 s (∗), and 50 s (■); (b) ($\dot{\gamma}$ = 15 s^{-1}, Wi_s = 4) for 4 s (□), 6 s (Δ), 8 s (▽), 10 s (◊), 12 s (∗), and 14 s (■); (c) ($\dot{\gamma}$ = 30 s^{-1}, Wi_s = 8) for 1 s (□), 2 s (Δ), 3 s (▽), 4 s (◊), 5 s (∗), and 7 s (■).

unaltered[5] (Figure 1, micrograph 2[28]). For longer flow times, where a change in the slope is observed (curve 3), n decreases. Oriented shish-kebabs are formed by crystalline lamellae growing in two dimensions (2D) off fibrillar nuclei (Figure 1, micrograph 3[28]), for which it can be derived that $n = 2$ and $C = \pi NLG^2$, with L the total length of the shishes.[18,31] Also in this situation, no sporadic nucleation is expected. Of course, not only fibrillar structures are formed, spherulites will grow as well, and thus $2 < n < 3$, as a function of time. For the experiments shown in Figure 1 the resulting morphologies were confirmed using optical microscopy (OM) and wide-angle X-ray diffraction (WAXD) (Hristova, D. G., personal communication, used in ref 23). To summarize the above, three morphology types are distinguished: (1) Quiescent crystallization: spherulites are formed by crystalline

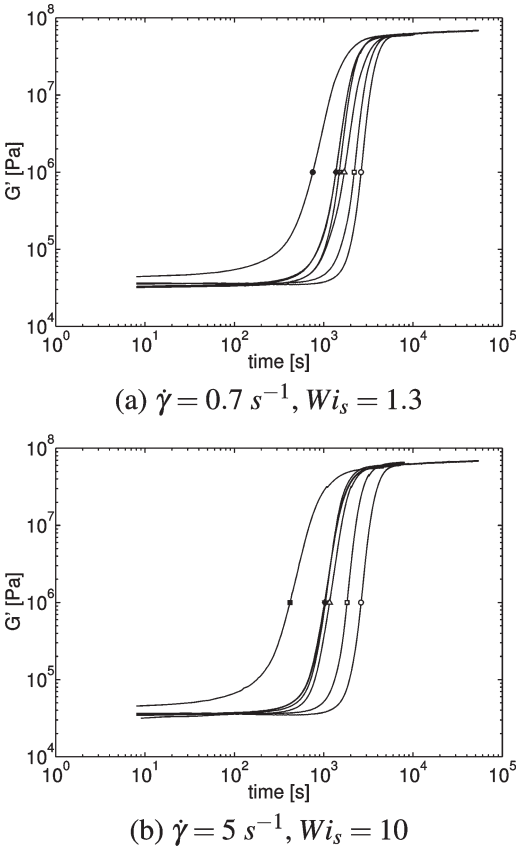

Figure 5. Time buildup of the storage modulus for iPP3 at T_c = 138 °C under quiescent conditions (○) and after flow application: (a) ($\dot{\gamma}$ = 0.7 s^{-1}, Wi_s = 1.3) for 50 s (□), 120 s (Δ), 150 s (▽), 180 s (◇), 200 s (∗), and 400 s (■); (b) ($\dot{\gamma}$ = 5 s^{-1}, Wi_s = 10) for 2 s (□), 8 s (Δ), 10 s (▽), 15 s (◇), 18 s (∗), and 50 s (■).

lamellae growing in three dimensions off pointlike nuclei, whose number density depends on the temperature. (2) Shift of modulus curve: the number density of pointlike nuclei increases with the strain rate and the duration of flow. This leads to a more fine-grained spherulitic morphology. (3) Shift and shape change: shish-kebabs are formed by crystalline lamellae growing in two dimensions off fibrillar nuclei, whose number density and length increase with strain rate and duration of flow.

On the basis of the rheology of the polymer, four flow regimes are defined by van Meerveld et al.,[16] and their interactions with the crystallization process are studied. The transitions between these regimes are defined by critical values of the Weissenberg number, Wi (= $\dot{\gamma}\tau$), related to molecular orientation and molecular stretch. Both orientation and stretch are characterized by a specific time scale: the reptation time, τ_{rep}, and the stretch relaxation time, or Rouse time, τ_s, respectively. In regime I, for Wi_{rep} and $Wi_s < 1$, the chains are in their equilibrium state, and flow has no effect on crystallization. The transition to regime II corresponds to orientation of the contour path ($Wi_{rep} > 1$, $Wi_s < 1$), which enhances the number density of pointlike nuclei. The onset of chain stretching ($Wi_{rep} > 1$, $Wi_s > 1$) marks regime III, and in the fourth and final regime, IV, the chains are strongly stretched, deviating from the Gaussian configuration, and the amount of rotational isomerization (RI) is large. Regime IV is reached when $\lambda > \lambda^*(T)$; i.e., the molecular stretch ratio λ has to be larger than a certain critical value $\lambda^*(T)$. On the basis of the analysis of FIC experiments reported in literature, it was concluded that the shish-kebab morphology develops when the HMW chains are subjected to the condition $Wi_s > 1$ for a sufficiently long time to fulfill the condition $\lambda > \lambda^*(T)$.[16]

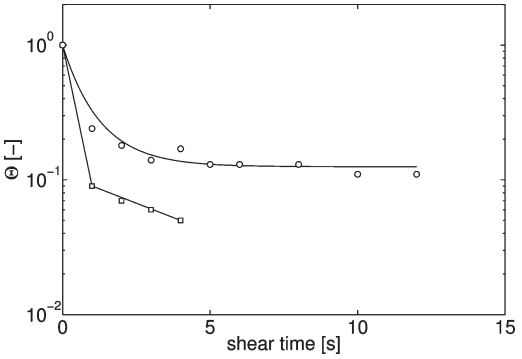

Figure 6. Normalized crystallization half-time, Θ, obtained from the dynamical mechanical experiments for iPP1, versus shear time: (○) $\dot{\gamma}$ = 20 s^{-1}, Wi_s = 1.3; (□) $\dot{\gamma}$ = 60 s^{-1}, Wi_s = 4.

4. Results and Discussion

4.1. DSC. The nominal melting temperature, T_m, the amount of crystallinity, X_c, determined from the melting enthalpy, ΔH_m, and the (peak) crystallization temperature, T_c, are given in Table 1. The materials are heterogeneously nucleated, different for the three grades, and hence small differences in T_m, X_c, and T_c are observed.

4.2. Rheological Properties. The rheological properties of the three iPP grades at a temperature of 220 °C are shown in Figure 2. The horizontal and vertical shift factors are listed in Table 2. An Arrhenius temperature dependence is found for the horizontal shift factor (a_T), and the vertical shift factor, b_T, shows no strong temperature dependence ($b_T \sim 1$). The measurements on grade iPP3 correspond well with those in ref 28. The relaxation time spectrum (at 220 °C) is calculated from the rheological properties using a discrete Maxwell relaxation time spectrum (g_i, τ_i):[33]

$$G'(\omega) = \sum_i g_i \frac{\omega^2 {\tau_i}^2}{1 + \omega^2 {\tau_i}^2} \tag{8}$$

$$G''(\omega) = \sum_i g_i \frac{\omega \tau_i}{1 + \omega^2 {\tau_i}^2} \tag{9}$$

The sets of relaxation moduli, g_i, and times, τ_i, are given in Table 2, which nicely fit the measured G' and G'' (solid lines in Figure 2). For iPP3, the reported relaxation spectrum is taken from Swartjes.[28] The common rule of 1.2−1.5 modes per decade in ω is applied to fit the modes to G' and G''. Care is taken that (a) the fastest mode is not outside the measured regime and (b) the slowest mode does not fall within the terminal zone. Furthermore, modes with similar modulus or relaxation time are combined to one mode. We also probed, without mentioning, fewer or more modes than the ones reported. Here, the modes that give the best fit are reported. Table 3 shows the longest relaxation time from the discrete spectrum, τ_{rep}^{HMW}, for the three grades at 138 °C, being the temperature at which the crystallization experiments are performed.

The transitions between the different flow regimes for FIC are defined by two characteristic Weissenberg numbers[16] based on the reptation time, τ_{rep}, and the Rouse, or stretch relaxation time, τ_s, defined as $Wi_{rep} = \dot{\gamma}\tau_{rep}$ and $Wi_s = \dot{\gamma}\tau_s$, respectively. The values of τ_s for the three materials can be estimated according to[34]

$$\tau_s = \tau_{rep}/3Z \tag{10}$$

with Z the average number of entanglements ($Z = M_w/M_e$). The values for the three grades are $Z_{iPP1} = 60$, $Z_{iPP2} = 70$, and $Z_{iPP3} = 122$, using a value of M_e = 5200 g mol^{-1} for iPP.[35]

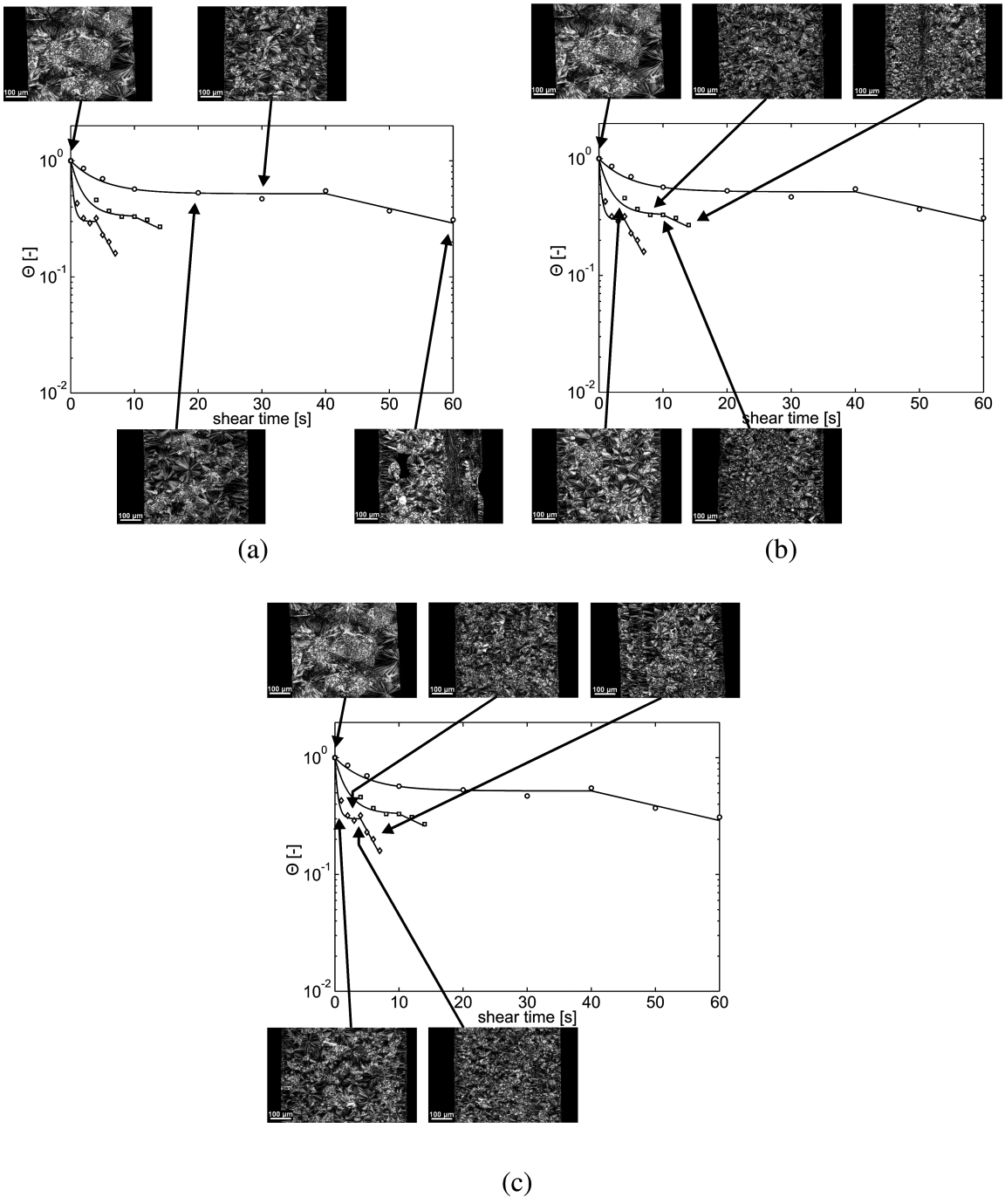

Figure 7. Normalized crystallization half-time, Θ, obtained from the dynamical mechanical experiments for iPP2, versus shear time: (○) $\dot{\gamma} = 5\ s^{-1}$, $Wi_s = 1.3$; (□) $\dot{\gamma} = 15\ s^{-1}$, $Wi_s = 4$; (◇) $\dot{\gamma} = 30\ s^{-1}$, $Wi_s = 8$. Micrographs show the final morphology at the edge of the sample for (a) $\dot{\gamma} = 5\ s^{-1}$, (b) $\dot{\gamma} = 15\ s^{-1}$, and (c) $\dot{\gamma} = 30\ s^{-1}$.

As there is strong experimental evidence that the high molecular weight (HMW) tail of the MWD dominates the FIC dynamics,[2,13−15] τ_{rep}^{HMW} is used as a measure for the HMW tail. When the terminal zone is visible in the rheology of a material, the longest relaxation time is the inverse of the frequency at which the slopes of G' and G'' deviate from 2 and 1, respectively, which is the case for iPP1 and iPP2. For iPP3, the terminal regime could not be determined, and the longest relaxation time from the spectrum underestimates the true value for the longest chains giving a measurable response. However, since we want to perform the FIC experiments in the flow regime where oriented structures are expected, this underestimation of τ_{rep}^{HMW} leads to an overestimation of the critical value of $\dot{\gamma}$, marking the beginning of the stretching regime, and consequently, the applied shear rate will certainly lie in regime III. The values for τ_s^{HMW} corresponding to τ_{rep}^{HMW} are listed in Table 3 together with the characteristic shear rates for the transitions between the orientation and stretch regimes.

4.3. Flow-Induced Crystallization Experiments. In the experiments the isothermal crystallization temperature, T_{exp}, is set to 138 °C. In order to investigate when fibrillar structures form, the shear rate $\dot{\gamma}$ has to be at least as high as $\dot{\gamma}_{II\rightarrow III}$ (Table 3) to guarantee $Wi_s \geq 1$. For $Wi_s = 1.3$ the values of the critical shear rate are 20, 5, and 0.7 s^{-1}, for iPP1, iPP2, and iPP3, respectively. Although a plate−plate configuration is used, with the consequence that the shear rate increases

linearly from 0 s^{-1} in the center of the plate to the set $\dot{\gamma}$ at the edge, leading to a gradient in crystallization kinetics over the radius, the response of G' is mainly governed by changes in the outermost part of the sample, where the conditions are prescribed, since the measured torque scales with the radius cubed. For the further analysis the shear rates mentioned, are the prescribed shear rates at the edge. The evolution of G' measured under quiescent conditions and after application of flow (fixed shear rate and varying flow times) is shown in Figure 3a, Figure 4a, and Figure 5a for iPP1, iPP2, and iPP3 (Wi_s=1.3), respectively. Applying a shear flow accelerates the crystallization process. The important observations that can be made from these results are as follows:

- For iPP1 (narrow MWD) only an effect on the time of onset of the crystallization process is observed. The shape of the evolution profile of the storage modulus does not change with increasing flow time, which implies no change in (the type of) crystallization kinetics, at least up to the maximum shear time of 12 s, which is the limiting time for $\dot{\gamma} = 20\ s^{-1}$ to have a stable experiment. The acceleration of the crystallization process becomes independent of shear time between $t_s = 2$ s and $t_s = 6$ s.
- For iPP2 and iPP3 (medium to broad MWD) the crystallization rates are increased with longer shear times, followed by a region that is unaffected with an increase in shear time as observed in iPP1, which is ascribed to a saturation of pointlike nuclei. Only for shear times above 40 and 200 s, respectively, the crystallization process is accelerated again, linked to a change in kinetics, observed from a change in the slope and a rise of the initial G' plateau (iPP3 only).

The effect of higher shear rates is investigated as well. For iPP1 the second set of experiments is performed at a shear rate of 60 s^{-1} ($Wi_s = 4$), for iPP2 $\dot{\gamma} = 15$ ($Wi_s = 4$) and 30 s^{-1} ($Wi_s = 8$), and for iPP3 a shear rate of 5 s^{-1} is chosen corresponding to a Wi_s of 10; see Figure 3b, Figure 4b,c, and Figure 5b. For iPP1 application of 1 s of flow speeds up the crystallization process without changing the kinetics, but the results for a flow time of 2 s and higher show a gradual change in the slope, which implies a change in morphology. The saturation in iPP1 under strong flow conditions is apparently obscured by the transition to oriented crystal growth. For iPP2 and iPP3 similar observations are made compared to $Wi_s = 1.3$, where saturation of pointlike nucleation is clearly observed before the transition to oriented growth. The physics behind this phenomenon will be investigated in the near future. One might speculate that the melt simply runs out of sufficiently long chains. This means that there is a critical molecular weight, depending on the temperature and the flow rate, as already suggested for thread-like nuclei.[13,36]

The effectiveness of flow is quantified by defining a normalized crystallization half-time, Θ, as[37]

$$\Theta = \frac{t_{1/2,\dot{\gamma}}}{t_{1/2,Q}} \tag{11}$$

with $t_{1/2}$ the time at which half of the change in viscoelastic functions occurs. The FIC experiments are indicated by the subscript $\dot{\gamma}$ while Q indicates the half time for quiescent conditions. To calculate $t_{1/2}$, the G' data are normalized to estimate the degree of space filling, following Pogodina et al.:[4]

$$\phi_P = \frac{\log G' - \log G'_0}{\log G'_1 - \log G'_0} \tag{12}$$

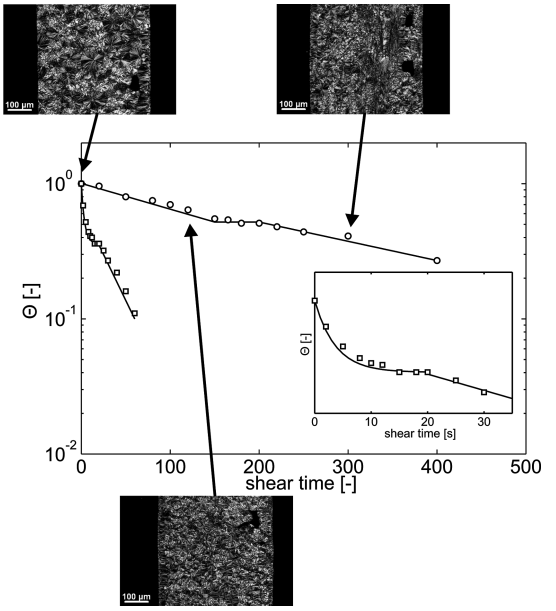

Figure 8. Normalized crystallization half-time, Θ, obtained from the dynamical mechanical experiments for iPP3, versus shear time: (○) $\dot{\gamma} = 0.7\ s^{-1}$, $Wi_s = 1.3$; (□) $\dot{\gamma} = 5\ s^{-1}$, $Wi_s = 10$. The inset shows the saturation plateau for $\dot{\gamma} = 5\ s^{-1}$. Micrographs show the final morphology at the edge of the sample for $\dot{\gamma} = 0.7\ s^{-1}$.

with G'_0 and G'_1 the values of the start and end plateau, respectively. The end plateau is not horizontal because of secondary crystallization. Therefore, G'_1 is defined as the intercept of the tangents drawn along the extrapolated end plateau and the regime of fastest increase in G'. The influence of shear time on Θ is shown in Figures 6, 7, and 8 for iPP1, iPP2, and iPP3, respectively. For iPP1 sheared at $\dot{\gamma} = 20\ s^{-1}$, saturation is reflected by the presence of the plateau, where Θ is unaffected by the shear time. In this plateau regime the kinetics do not change with respect to those under quiescent conditions (Figure 3). For the higher shear rate (60 s^{-1}), we observe a strong decrease in Θ at 1 s of flow time, followed by a more gradual, but steady, decrease for longer shear times without any saturation. For iPP2, the behavior of Θ is similar for the three flow conditions applied (Figure 7): First, a region of acceleration of the crystallization process, that proceeds into the saturation plateau, followed by a second speed-up linked to a change in kinetics, i.e., the transition to oriented crystal growth. The HMW grade, iPP3, shows similar results (see Figure 8), and although the plateau ($Wi_s = 1.3$) is not as clear as for iPP1 and iPP2, it is still present. The inset in Figure 8 clarifies the evolution of Θ with shear time at an increased $\dot{\gamma}$ (5 s^{-1}, $Wi_s = 10$). For all grades, the lower value of $\dot{\gamma}$ is set above the critical value for being in the stretch regime ($Wi_s = 1.3$). However, iPP1 shows no change in crystallization kinetics and no decrease of Θ after the saturation plateau. This could be because the limiting flow time of 12 s is still not long enough to stretch the molecules above $\lambda^*(T)$.[38] Another possible explanation is that $\dot{\gamma}$ is still too low to be in the stretch regime. Van Meerveld et al.[16] concluded that to be in this regime $Wi_s > 1-10$. The critical shear rate is calculated here from $Wi_s = 1$, so it is the lower limit to the prerequisite, and it might not be sufficient to stretch even the longest chains present in iPP1.

Postmortem cuts are made of iPP2 and iPP3 samples for several processing conditions as close as possible to the edge where the conditions are prescribed. The micrographs are included in Figures 7 and 8. It can easily be recognized that all spherulites have the same size, indicating that they are all

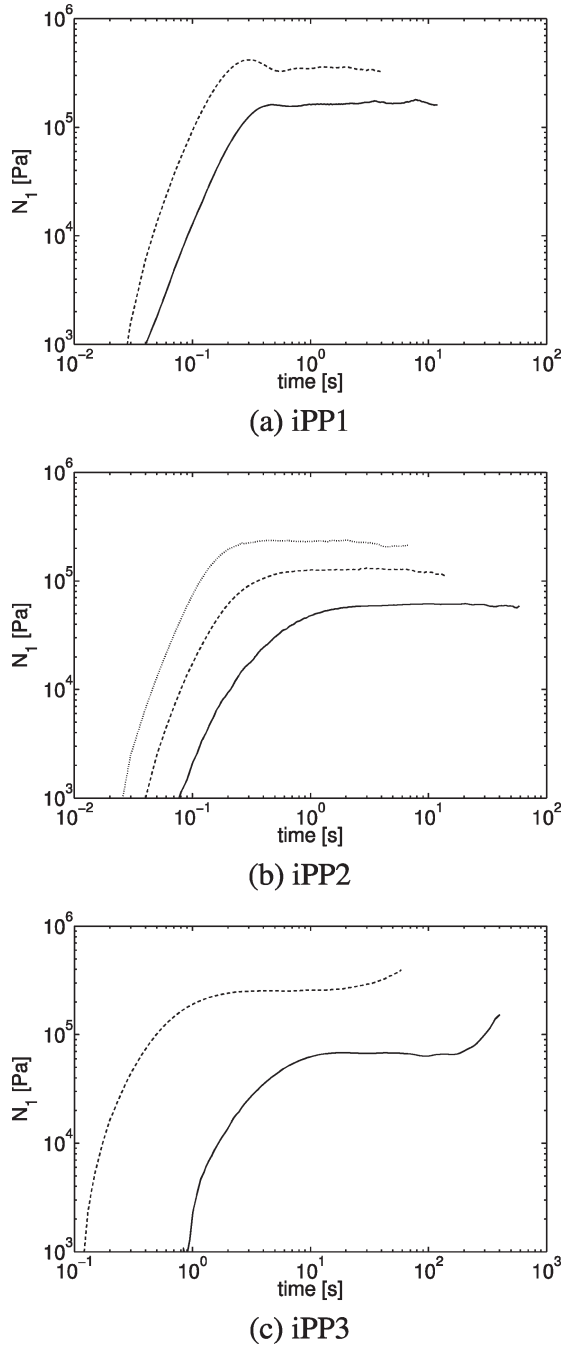

Figure 9. First normal stress difference, N_1, during flow for the highest shear time at every shear rate applied for iPP1 (a), iPP2 (b), and iPP3 (c). Solid line: $Wi_s = 1.3$ in all cases; dashed line: $Wi_s = 4$ for iPP1 and iPP2, $Wi_s = 10$ for iPP3; dotted line: $Wi_s = 8$ for iPP2.

formed at the same time. Small differences in size depend on the position in the spherulite; i.e., a spherulite which is cut in the middle shows the largest cross section, whereas the cross section of a spherulite cut slightly above or below the middle is smaller. Furthermore, with increasing shear rate the number of nuclei increases up to the saturation plateau, observed as more and smaller spherulites, but the size for a given condition is almost constant. In the saturation plateau, where the crystallization process is unaffected by an increase in flow time, the size of the spherulites is similar for different flow times. For conditions that result in a change in kinetics after saturation the micrographs show indeed the presence of fibrillar structures. The postmortem cuts thus confirm that there is no sporadic nucleation (at least after short-term shear) and hence that the Avrami equation (eq 2) can be used, up to this change, to determine the number of nuclei from these rheological crystallization experiments.

Table 4. Cross Model Parameters at $T = 138$ °C

	iPP1	iPP2	iPP3
η_0 [Pa·s]	9366	7668	72944
K [s]	0.216	0.310	5.873
n	0.33	0.38	0.38

Flow-induced crystallization was monitored using birefringence,[8,12] which, at start-up of flow, first showed a slight overshoot, related to chain stretching, followed by a plateau before it relaxes back completely after cessation of flow. An upturn from the transient birefringence plateau is observed for longer shear times, which arises due to the formation of oriented structures, and it does not decay to zero upon cessation of flow. Birefringence is related to the first normal stress difference, N_1, via the stress optical rule,[33] which is measured during flow. The N_1 traces of iPP3 are shown in Figure 9c, and most of the features observed in birefringence can be recognized: the start-up, but no detectable overshoot, followed by a plateau and an upswing at longer shear times. The shift in starting time arises from a negative N_1 at the start of shear due to shrinkage of the sample during cooling, which pulls the plates together. Although the gap is adjusted for shrinkage during cooling to obtain a sample with a small edge meniscus, a small pulling force remains. It should be noticed that the time at which the upswing occurs is equal to shear time at which a change in crystallization kinetics is observed, i.e., a shape change of $G'(t)$ (Figure 5), and where the plateau in Θ ends (Figure 8). For iPP1 and iPP2 the first normal stress difference is displayed in Figures 9a and 9b, respectively. The N_1 traces show no upswing, even at longer flow times, for which a change in crystallization kinetics is observed from the evolution of G'. It is argued that for iPP1 and iPP2 the flow time is still too short to show the upswing. Baert et al.[12] found, also for experiments without an upswing in birefringence, a transition to oriented structures generated during shear, which occurred when the birefringence, and thus N_1, did not completely relax back to zero.

4.4. Critical Work. The deformation history experienced by the polymer molecules, which is the result of a (sometimes complex) combination of shear rate and shear time, is known to influence the crystallization kinetics. One of the combinations is *mechanical work* as defined in eq 1 by Janeschitz-Kriegl et al.[19] An enormous increase in the number of point nuclei was observed with increasing amount of work. At high amounts of applied work a transition to threadlike nuclei occurred. Mykhaylyk et al.[20] showed that, above a critical shear rate, equal to the inverse of the Rouse time associated with the longest chains, the amount of work necessary to create oriented structures is independent of the shear rate. Since the FIC experiments are performed at shear rates above the critical value for chain stretch, it is investigated here whether the changes in the crystallization kinetics observed relate to a critical value of applied work. The shear rate applied is constant and the transient start-up is short compared to the total flow time (see e.g. Figure 9). Therefore, the equation for total applied work (eq 1) is transformed into

$$w = \eta(\dot{\gamma})\dot{\gamma}^2 t_s \tag{13}$$

The values for $\eta(\dot{\gamma})$ are derived from the complex viscosity, $\eta^*(\omega)$, at $T = 138$ °C applying the Cox−Merz rule. A Cross model describes $\eta^*(\omega)$ (eq 14), with η_0 the zero shear

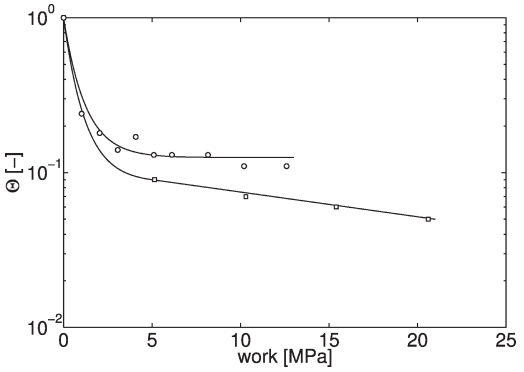

Figure 10. Θ versus work for iPP1: (○) $\dot{\gamma} = 20\ s^{-1}$, $Wi_s = 1.3$; (□) $\dot{\gamma} = 60\ s^{-1}$, $Wi_s = 4$.

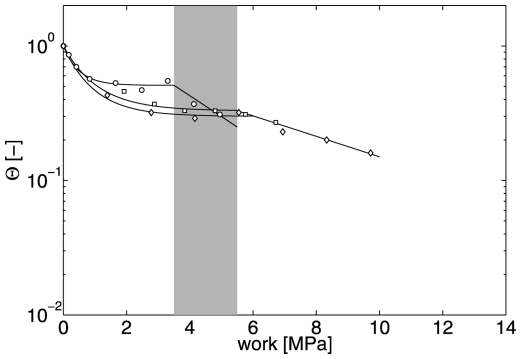

Figure 11. Θ versus work for iPP2: (○) $\dot{\gamma} = 5\ s^{-1}$, $Wi_s = 1.3$; (□) $\dot{\gamma} = 15\ s^{-1}$, $Wi_s = 4$; (◇) $\dot{\gamma} = 30\ s^{-1}$, $Wi_s = 8$.

viscosity, K a time constant, and m the power-law index. The parameter values are given in Table 4.

$$\eta^*(\omega) = \frac{\eta_0}{1+(K\omega)^{1-m}} \tag{14}$$

For all flow conditions, thus all Wi, the normalized transition half-time as a function of work is shown in Figure 10 (iPP1), Figure 11 (iPP2), and Figure 12 (iPP3). In case of iPP1, it is not possible to relate a work value to a change in the crystallization behavior, simply because no transition is observed in Figure 3a for $\dot{\gamma} = 20\ s^{-1}$. This could be because $Wi_s = 1.3$ is not high enough for iPP1. For $\dot{\gamma} = 60\ s^{-1}$ a change occurs between work values of 5 and 10 MPa, since at 1 s of flow ($w = 5$ MPa) crystallization kinetics do not change with respect to those under quiescent conditions (see Figure 3b), while the results for a flow time of 2 s ($w = 10$ MPa) and higher show a gradual change in the slope in Figure 3b, which implies a change in morphology (see Figure 1). The critical value for the amount of work should lie in between $5 < w_{crit} < 10$ MPa, but the experimental setup does not allow for flow durations between 1 and 2 s. Both iPP2 and iPP3 show a transition to oriented crystal growth for all Wi_s, which, in the case of iPP3, as explained in section 4.2, is underestimated. It is clear from Figure 11 and Figure 12 that in both cases the transition falls within a relatively narrow range of work values: 3.5−5.5 MPa and 2−4 MPa for iPP2 and iPP3, respectively, indicated by the gray area. Remarkably, these values are similar, while the difference in Wi_s is a factor 6 (iPP2) to 8 (iPP3). The results for these three materials clearly show that the amount of work necessary to create oriented structures decreases with molecular weight. Mykhaylyk et al.[20] prepared model linear−linear blends of hydrogenated polybutadienes (h-PBD) from low-polydispersity polymers of 1700 and 15 kg/mol with different concentrations of long chains for

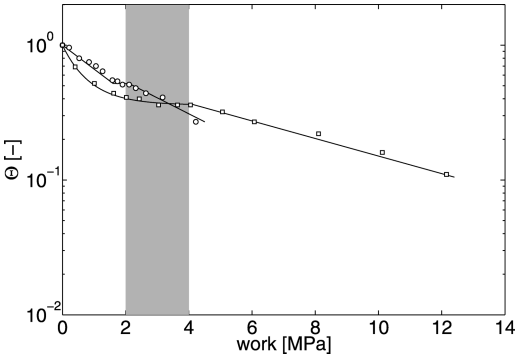

Figure 12. Θ versus work for iPP3: (○) $\dot{\gamma} = 0.7\ s^{-1}$, $Wi_s = 1.3$; (□) $\dot{\gamma} = 5\ s^{-1}$, $Wi_s = 10$.

Table 5. Parameters (Eqs 16 and 17) for the Effective Number of Nuclei, $N(T)$, and the Spherulitic Growth Rate, $G(T)$, for iPP1 and iPP2, Respectively

	iPP1	iPP2
N_{ref} [m^{-3}]	1.6×10^{14}	3.8×10^{13}
$T_{N,ref}$ [K]	383	383
c_N	0.118	0.115
G_{ref} [m s^{-1}]	4×10^{-6}	3×10^{-6}
$T_{G,ref}$ [K]	363	363
c_G	2.54×10^{-3}	2.3×10^{-3}

Table 6. Growth Rate, G, and Effective Number of Nuclei, N, at T = 138 °C for iPP1, iPP2, and iPP3

	iPP1	iPP2	iPP3
G [m s^{-1}]	2×10^{-8}	1.5×10^{-8}	1.5×10^{-8}
N [m^{-3}] (OM, eq 16)	5×10^{12}	1.5×10^{12}	1.2×10^{12}
N [m^{-3}] (eqs 20, 22)	8.2×10^{10}	4.2×10^{11}	3.3×10^{12}

their FIC experiments (at $T = 115$ °C). They found that, for shear rates above the inverse Rouse time of the long chains, a critical amount of work, w_{crit}, was needed to form oriented structures. The critical amount is independent of the shear rate (up to $\dot{\gamma} = 90\ s^{-1}$) and depends on the concentration of long chains, i.e., for concentrations of 0.5, 2, and 4 wt % HMW polymer, $w_{crit} = 7.8 \pm 0.07$, 2.38 ± 0.07, and 0.80 ± 0.13 MPa, respectively. Hence, our results are in qualitative agreement with those of Mykhaylyk et al.[20]

The rheological classification is only valid for short-term shear experiments. For longer shear times, precursors/nuclei start to arise during flow, which act as local physical cross-links, causing the longest rheological relaxation time to increase, which explains the so-called self-enhancing effect.[21] For high Wi_s, the shear times are definitely short compared to the quiescent onset time for crystallization (>1000 s), and the experiments fall within the definition of short-term shear. For iPP2 it can be clearly seen (Figure 11) that the "critical" work value for $Wi_s = 4$ and $Wi_s = 8$ is the same (5.5 MPa). In case of $Wi = 1.3$, for all materials, the work necessary to see the transition from an isotropic to an oriented morphology is much lower. We believe that in these cases the local cross-linking effect plays a role, and precursors/nuclei that are formed during shear alter the rheology of the material. Because of an increase in the longest rheological relaxation time, it becomes easier to orient and stretch the chains and to form fibrillar nuclei (shishes). In other words, less work (calculated, based on the initial melt rheology) is needed to form fibrillar nuclei.

4.5. Determination of Number of Quiescent Pointlike Nuclei. In the experiments, the undercooled melt is subjected to a short, well-defined shear flow in the early stage of

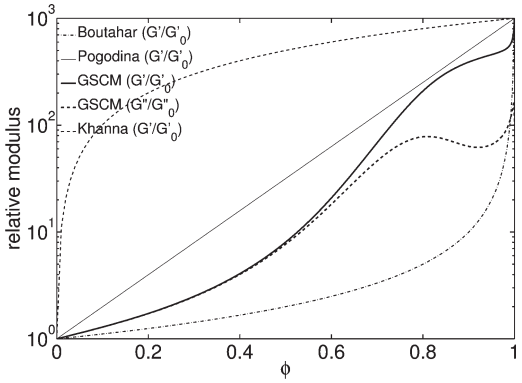

Figure 13. Relative modulus ($G'_1/G'_0 = 10^3$, $G''_1/G''_0 = 10^2$) versus space filling calculated according to Boutahar et al.[39] (eq 18), Khanna[41] (eq 19), Pogodina et al.[47] (eq 12), and Steenbakkers and Peters[23] (eq 20) for G' and G''.

crystallization, where nearly all material is still in the amorphous phase. For spherulites, the Avrami equation describes space filling, ϕ, in case of isothermal crystallization, for which all nuclei, N, appear at the same time, t_0, and the growth rate, G, is constant in time:[30,31]

$$\phi = 1 - \exp\left[-\frac{4}{3}\pi N G^3 (t - t_0)^3\right] \tag{15}$$

If a polymer crystallizes during application of flow, both N and G are influenced by the flow (see e.g. ref 9). In our experiments nucleation takes place during flow, but the growth process occurs after cessation of flow. Hence, the growth rate remains unaltered.[5] The measured values for N and G of iPP1 and iPP2 for quiescent conditions and temperatures between 80 and 120 °C were provided by Dr. M. Gahleitner (Borealis, Linz) and determined in the group of Prof. Eder at J. Kepler University (Linz), and for iPP3 the number of nuclei and growth rates are determined in a temperature range of 125−147 °C:[28] $N_{iPP3} = 1.2 \times 10^{12}$ m^{-3} and $G_{iPP3} = 1.5 \times 10^{-8}$ m s^{-1} at $T = 138$ °C. For iPP1 and iPP2, the N and G values at 138 °C are described with two exponential functions:[21]

$$N(T) = N_{ref} \exp[-c_N(T - T_{N,ref})] \tag{16}$$

$$G(T) = G_{ref} \exp[-c_G(T - T_{G,ref})^2] \tag{17}$$

in which N_{ref} is the number of nuclei at the reference temperature, $T_{N,ref} = 383$ K, and G_{ref} is the growth rate at $T_{G,ref} = 363$ K. The parameter values are given in Table 5. At the experimental temperature of 138 °C the values for N and G for iPP1 equal $N_{iPP1} = 5 \times 10^{12}$ m^{-3} and $G_{iPP1} = 2 \times 10^{-8}$ m s^{-1}, and for iPP2 $N_{iPP2} = 1.5 \times 10^{12}$ m^{-3} and $G_{iPP2} = 1.5 \times 10^{-8}$ m s^{-1}. The growth rates for the three grades, summarized in Table 6, are almost equal, but the difference in number of nuclei is a factor 3 to 4. According to Avrami, under quiescent conditions iPP1 should crystallize faster than the other two iPPs by at least a factor of 2 given the crystallization half-times, determined with eq 15. However, the measurements show that both iPP2 and iPP3 are faster than iPP1, i.e., $t_{1/2,iPP1}/t_{1/2,iPP2} = 1.35$ and $t_{1/2,iPP1}/t_{1/2,iPP3} = 2.65$, when a logarithmic scaling law (eq 12) is applied. For iPP2 and iPP3 the rheological measurements and the Avrami model correspond rather well; thus, in both cases the $t_{1/2}$ values are comparable. However, for iPP1 the mismatch is quite large; Avrami predicts a 4.5 times faster crystallization than what the experiments show. The rheological measurements are confirmed by DSC experiments under the same conditions, showing a similar time evolution of crystallinity. The values for N and G, used in the Avrami equation, are obtained from exponential fits (eqs 16 and 17) to the low-temperature data, which can yield errors. This could explain the mismatch found. Therefore, we collected growth rate data for several different iPP grades, and one general master curve for G was obtained as long as the material crystallizes in the α-form.[18,24] The measured growth rate data for iPP1, iPP2, and iPP3 all nicely fit on this curve. Therefore, we expect that the G value for iPP1 is correctly described by eq 17. To describe both the rheometry and DSC measurements for iPP1 and using $G_{iPP1} = 2\,10^{-8}$ m s^{-1}, we need a value of $N \sim 5 \times 10^{10}$ m^{-3} for the number of nuclei, which is $O(100)$ times lower than the value obtained from eq 16. We will use this new lower value in the remainder of this paper.

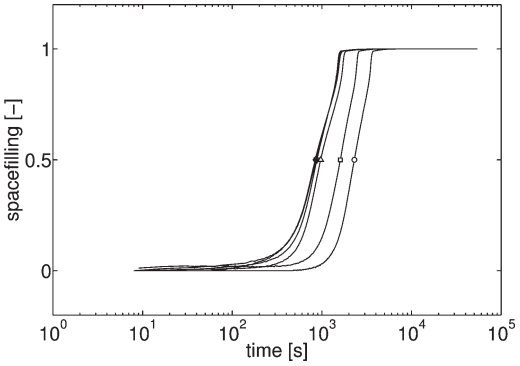

Figure 14. Space filling for iPP3 at $T_c = 138$ °C for quiescent conditions (○) and after flow application ($\dot{\gamma} = 5$ s^{-1}, $Wi_s = 10$) for 2 s (□), 8 s (Δ), 10 s (▽), 15 s (◇), and 18 s (∗).

4.6. Number of Flow-Induced Nuclei from Rheometry. Rheometry has been established as an adequate probe of space filling, at least for crystallizing melts with a suspension-like morphology. Care should be taken when interpreting rheological data such as $G'(t)$ and $G''(t)$ for samples with a very fine-grained (colloidal or gel-like) morphology, which is promoted for example by fast cooling and by the presence of nucleating agents. Boutahar et al.[39] compared the evolution of linear viscoelastic properties of both kinds of crystallizing melts. For a suspension-like polypropylene, they calculated the degree of space filling as follows:

$$\phi_B = 1 - \frac{G'_0}{G'} \tag{18}$$

They also did DSC experiments. The linearly normalized, time-integrated heat flow was shown to agree with the space filling obtained from polarized optical microscopy.[40] Equation 18 was close to the DSC result up to $\phi \approx 0.4$ but overpredicted it in the later stages of crystallization.[39]

A more widespread empirical relation is

$$\phi_K = \frac{G' - G'_0}{G'_1 - G'_0} \tag{19}$$

which is usually referenced to Khanna[41] (despite being used earlier by Gauthier et al.[42]) and predicts much lower degrees of space filling than eq 18 over nearly the whole range of measured storage moduli. For example, if $G'/G'_0 = 10$, eq 18 gives $\phi = 0.9$, whereas eq 19 gives $\phi = 9(G'_1/G'_0 - 1)^{-1}$. Since the ratio of the phases' storage moduli is typically between 10^3 and 10^4 (see Figures 3−5), the predicted space filling is then in the order of 10^{-3}−10^{-2}. This is shown in Figure 13.

Steenbakkers and Peters[23] used a linear viscoelastic version of the three-dimensional generalized self-consistent method (3D GSCM) of Christensen and Lo.[43−45] As input, they took the degree of space filling from optical microscopy and the plateau values of the dynamic moduli from oscillatory shear measurements. The calculated $G'(t)$ and $G''(t)$

agreed very well with experimental data, except for melts with a long duration of shear flow before crystallization (probably due to oriented crystallization). Equation 19 was shown to overpredict $G'(t)$. The logarithmic normalization, eq 12, performed much better, though not as well as the 3D GSCM. Figure 13 shows that the relative storage modulus for a given degree of space filling, and vice versa, according to both methods lies in between eqs 18 and 19.

Steenbakkers and Peters applied the 3D GSCM to the experiments of Boutahar et al.[39,40] The degrees of space filling, obtained by fitting the model to the rheological data, were reasonably close to those of Boutahar et al. from DSC. However, the low-frequency behavior could not be described. Fitting similar data of Coppola et al.[46] lead to the same conclusion. For an isotactic polypropylene similar to iPP2, Pogodina et al.[47] observed this gel-like behavior below $\omega = 1$ rad s^{-1}. At the frequency of our experiments, $\omega = 5$ rad s^{-1}, it is safe to assume that the crystallizing melt can be modeled as a suspension.

Besides a three-dimensional (3D) also a two-dimensional (2D) model exists: the 3D GSCM gives the solution for spherical particles, the 2D version for long parallel cylindrical fibers, which allows to capture both the influence of spherulites and shish-kebab structures on the rheology. In the 3D case, the relative dynamic modulus, $f_G^* = G^*/G_0^*$, is obtained from

$$A^* f_G^{*2} + B^* f_G^* + C^* = 0 \tag{20}$$

with G^* the effective dynamic modulus and G_0^* the dynamic modulus of the continuous phase. The complex coefficients A^*, B^*, and C^* depend on $\phi, \mu^* = G_1^*/G_0^*$, which is the ratio of the complex moduli of the continuous phase (G_0^*) and dispersed phase (G_1^*), and ν_0 and ν_1, being the Poisson ratios of both phases. For the exact description of these coefficients, we refer to Christensen,[45] in which the elastic shear moduli have to be replaced by the complex moduli, and to the Appendix of Steenbakkers and Peters.[23] For long parallel cylindrical fibers in a matrix, the components of the fourth-order stiffness tensor, except the shear modulus in the transverse plane, were derived by Hashin and Rosen.[48] The relative dynamic longitudinal shear modulus, G_{12}^*/G_0^*, which is the relevant one for FIC in shear, because shish kebabs are usually perfectly aligned in the flow direction, is given by

$$f_{G_{12}}^* = \frac{G_{12}^*}{G_0^*} = \frac{(1+\phi)\mu^* + 1 - \phi}{(1-\phi)\mu^* + 1 + \phi} \tag{21}$$

and the relative transverse shear modulus, G_{23}^*/G_0^*, is given by the 2D GSCM, which is the same as eq 20, but with different definitions of the complex coefficients.[23,45]

The evolution of G' in the FIC experiments shows, up to and including the saturation plateau, similar behavior as the quiescent case, and therefore the 3D suspension model is used to derive space filling. Beyond the saturation plateau, the crystallization kinetics change; thus both spherical and cylindrical objects start to grow, and combined 2D/3D suspension modeling is necessary to adequately describe the experiments. One can imagine that, for every value of G', there exists an infinite number of possible combinations of volume fractions of the unoriented spherical particles, the oriented cylindrical particles and the continuous matrix phase. Determination of the proper combination is not possible (for now), and therefore, we restrict the analysis to the experiments that can be modeled solely with the 3D suspension model. In Figure 14, space filling derived from the dynamic moduli of iPP3 (Figure 5b) is given, except for the 50 s of shear time. The times for $\phi = 0.5$ are lower than

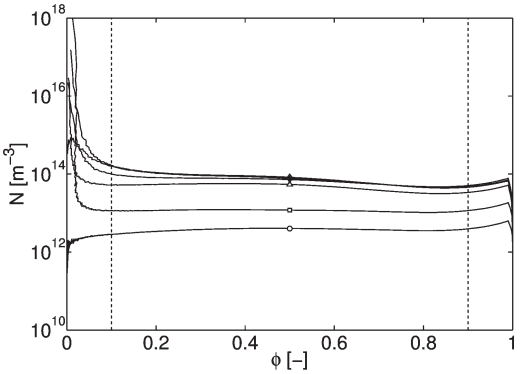

Figure 15. Number of pointlike nuclei for iPP3 at $T_c = 138$ °C derived from ϕ (Figure 14) using Avrami (eq 22) for quiescent conditions (○) and after flow application ($\dot{\gamma} = 5$ s^{-1}, $Wi_s = 10$) for 2 s (□), 8 s (Δ), 10 s (▽), 15 s (◊), and 18 s (∗).

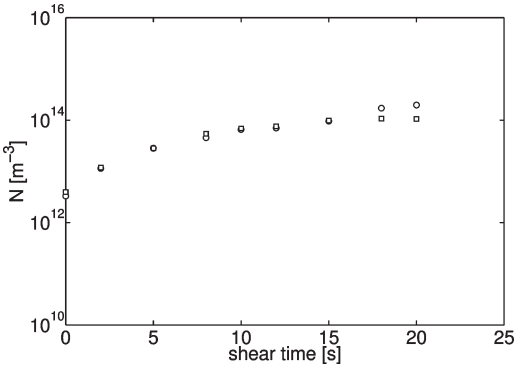

Figure 16. Number of pointlike nuclei for iPP3 at $T_c = 138$ °C derived from ϕ (Figure 14) using Avrami (eq 22): N_{avg} (○) and $N_{1/2}$ (□).

the $t_{1/2}$ values from the logarithmic scaling law (eq 12), but the resulting normalized half-time Θ (eq 11) does not change. With the assumption that all nuclei are present at $t_0 = 0$, the number of nuclei is estimated from space filling using the Avrami equation (eq 15, $G = 1.5 \times 10^{-8}$ m s^{-1}):

$$N = \frac{-3 \ln(1-\phi)}{4\pi G^3 t^3} \tag{22}$$

and shown in Figure 15. It is observed that N is almost constant between $\phi \approx 0.1$ and $\phi \approx 0.9$. The deviation at low and high ϕ values can be explained from variations in G_0^* and G_1^* among the experiments. For modeling, the plateau values of the quiescent case are used for all experiments, and a small increase in G_0^* for a different experiment leads to a strong increase in space filling and, consequently, Avrami then predicts an enormous number of nuclei. The evolution of space filling shows a sharp transition at $\phi = 1$ (see Figure 14), while the transition is more smooth with Avrami, resulting in a sudden drop in N. The number of nuclei is determined in two ways: (i) averaging between $\phi = 0.1$ and 0.9, N_{avg}, and (ii) taking the value at which $\phi = 0.5$, $N_{1/2}$. Both values compare well, only close to the transition to a change in crystallization kinetics a small difference is observed (see Figure 16). For the quiescent experiment $N_{avg} = 3.3 \times 10^{12}$ m^{-3} and $N_{1/2} = 3.9 \times 10^{12}$ m^{-3}, which is ≈3 times as large as measured.[28] However, the scattering in measured N is large ($6 \times 10^{11} < N < 2 \times 10^{12}$ m^{-3} at $T = 138$ °C). Furthermore, eq 15 is sensitive to the growth rate, i.e., a factor of 2 increase in G gives a factor of 8 decrease in N, to obtain the same evolution of ϕ. With $G = 2 \times 10^{-8}$ m s^{-1}, N_{avg} and $N_{1/2}$ become 1.6×10^{12} m^{-3} and 1.7×10^{12} m^{-3}, respectively.

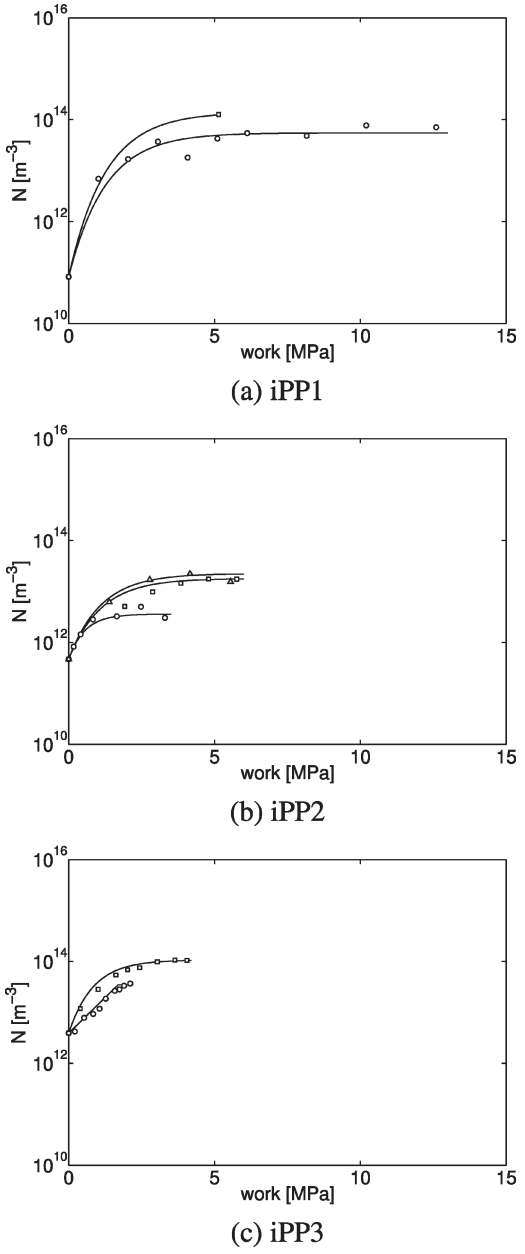

Figure 17. Number of pointlike nuclei ($N_{1/2}$) for (a) iPP1 (○: $\dot{\gamma} = 20\ s^{-1}$, $Wi_s = 1.3$/□: $\dot{\gamma} = 60\ s^{-1}$, $Wi_s = 4$), (b) iPP2 (○: $\dot{\gamma} = 5\ s^{-1}$, $Wi_s = 1.3$/□: $\dot{\gamma} = 15\ s^{-1}$, $Wi_s = 4$/Δ: $\dot{\gamma} = 30\ s^{-1}$, $Wi_s = 8$), and (c) iPP3 (○: $\dot{\gamma} = 0.7\ s^{-1}$, $Wi_s = 1.3$/□: $\dot{\gamma} = 5\ s^{-1}$, $Wi_s = 10$).

The number of nuclei, determined from all FIC experiments of the three grades suitable for 3D suspension modeling are summarized in Figure 17 using a crystal growth rate of $2 \times 10^{-8}\ m\ s^{-1}$ for iPP1 (Figure 17a) and $1.5 \times 10^{-8}\ m\ s^{-1}$ for iPP2 (Figure 17b) and iPP3 (Figure 17c). In general, flow strongly enhances the formation of pointlike nuclei. The number of nuclei under quiescent conditions for iPP1 ($\sim 1 \times 10^{11}\ m^{-3}$) compares well to the value determined from the $t_{1/2}$ value mentioned earlier ($\sim 5 \times 10^{10}\ m^{-3}$). For iPP2, it is only a factor 3 lower than the value from the fit on measured nucleation densities, due to either a difference between the real unknown quantity and the result from the exponential fit on the rather scattered data or the sensitivity of eq 15 to G. Again a saturation plateau is approached for all three grades at high values of work, depending on the flow conditions applied. Janeschitz-Kriegl et al.[19] did not observe any saturation but only a steady increase up to values of $N \sim 10^{16}$ with increasing amount of applied work, which is high compared to our results. Differences can arise from the fact that they used a different setup and that they count the number after the experiment from several optical micrographs. Figure 17 shows that for one iPP grade at the same level of applied work, but with a different shear rate, different quantities of nuclei are formed. However, the results for iPP2 suggest that, if Wi_s is not too close to 1, the same nucleation density is obtained at the same amount of work.

5. Conclusions

The FIC behavior of three polydisperse isotactic polypropylenes is examined using rheometry. The flow applied, with a shear rate above the critical value for the creation of oriented structures, first leads to an accelerated crystallization, which continues into a saturation with increasing flow time. Only after this saturation, the crystallization kinetics changes, leading to a second acceleration. Based on the observations, the acceleration regime 1 corresponds to an increase in the number of pointlike nuclei, and this number saturates with longer flow durations. Above a critical flow time, crystallization speeds up again corresponding to an altered growth mechanism, which is the formation of oriented nuclei. The second transition point relates well to a critical work value in the case of iPP2 and iPP3. For iPP1 the critical value is not clear but has to be at least higher than that of the HMW grade iPP3. The amount of applied work for the formation of fibrillar structures decreases with increasing molecular weight. It is shown that, with the aid of a suspension model, the number of flow-induced point nuclei can be derived. The main advantages of rheometry to obtain the number of nuclei over optical microscopy are (i) better reproducibility (±15% on N), while the scatter in N is much higher using OM,[5,28,49] and (ii) the applicability for filled systems when OM cannot be applied. Furthermore, with rheometry the response (G') comes from the complete sample, while in OM the viewing area is small, making it difficult to find a part representative for the whole sample.

Acknowledgment. This work is part of the Research Programme of the Dutch Polymer Institute (DPI), PO Box 902, 5600 AX Eindhoven, The Netherlands, project no. 454. The authors thank Pauline Schmit from the Department of Chemical Engineering and Chemistry, Polymer Technology (SKT), Eindhoven University of Technology, for the postmortem cuts and optical micrographs.

References and Notes

(1) Liedauer, S.; Eder, G.; Janeschitz-Kriegl, H.; Jerschow, P.; Geymayer, W.; Ingolic, E. *Int. Polym. Proc.* **1993**, *VIII*, 236–244.
(2) Vleeshouwers, S.; Meijer, H. E. H. *Rheol. Acta* **1996**, *35*, 391–399.
(3) Vega, J. F.; Hristova, D. G.; Peters, G. W. M. *J. Therm. Anal. Calorim.* **2009**.
(4) Pogodina, N. V.; Winter, H. H.; Srinivas, S. *J. Polym. Sci., Part B: Polym. Phys.* **1999**, *37*, 3512–3519.
(5) Koscher, E.; Fulchiron, R. *Polymer* **2002**, *43*, 6931–6942.
(6) Somani, R. H.; Hsiao, B. S.; Nogales, A.; Srinivas, S.; Tsou, A. H.; Sics, I.; Balta-Calleja, F. J.; Ezquerra, T. A. *Macromolecules* **2000**, *33*, 9385–9394.
(7) Baert, J.; van Puyvelde, P. *Polymer* **2006**, *47*, 5871–5879.
(8) Kumaraswamy, G.; Issaian, A. M.; Kornfield, J. A. *Macromolecules* **1999**, *32*, 7537–7547.
(9) Jay, F.; Haudin, J. M.; Monasse, B. *J. Mater. Sci.* **1999**, *34*, 2089–2102.
(10) Tribout, C.; Monasse, B.; Haudin, J. M. *Colloid Polym. Sci.* **1996**, *274*, 197–208.
(11) Langouche, F. *Macromolecules* **2006**, *39*, 2568–2573.
(12) Baert, J.; van Puyvelde, P.; Langouche, F. *Macromolecules* **2006**, *39*, 9215–9222.
(13) Keller, A.; Kolnaar, H. W. H. Flow-induced orientation and structure formation. In *Processing of Polymers*; Meijer, H., Ed.; Wiley-VCH: Weinheim, 1997; Vol. *18*, pp 189−268.

(14) Lagasse, R. R.; Maxwell, B. *Polym. Eng. Sci.* **1976**, *16*, 189–199.
(15) Seki, M.; Thurman, D. W.; Oberhauser, J. P.; Kornfield, J. A. *Macromolecules* **2002**, *35*, 2583–2594.
(16) van Meerveld, J.; Peters, G. W. M.; Hütter, M. *Rheol. Acta* **2004**, *44*, 119–134.
(17) Elmoumni, A.; Winter, H. H. *Rheol. Acta* **2006**, *45*, 793–801.
(18) Eder, G.; Janeschitz-Kriegl, H. Structure development during processing: crystallization. In *Processing of Polymers*; Meijer, H., Ed.; Wiley-VCH: Weinheim, 1997; Vol. 18 of Materials Science and Technology: a Comprehensive Treatment, pp 269−342.
(19) Janeschitz-Kriegl, H.; Ratajski, E.; Stadlbauer, M. *Rheol. Acta* **2003**, *42*, 355–364.
(20) Mykhaylyk, O. O.; Chambon, P.; Graham, R. S.; Fairclough, J. P. A.; Olmsted, P. D.; Ryan, A. J. *Macromolecules* **2008**, *41*, 1901–1904.
(21) Zuidema, H.; Peters, G.W. M.; Meijer, H. E. H. *Macromol. Theory Simul.* **2001**, *10*, 447–460.
(22) McHugh, A. J.; Guy, R. K.; Tree, D. A. *Colloid Polym. Sci.* **1993**, *271*, 629–645.
(23) Steenbakkers, R. J. A.; Peters, G. W. M. *Rheol. Acta* **2008**, *47*, 643–665.
(24) Lamberti, G. *Polym. Bull.* **2004**, *52*, 443–449.
(25) Gahleitner, M.; Jääskeläinen, P.; Ratajski, E.; Paulik, C.; Reussner, J.; Wolfschwenger, J.; Neissl, W. *J. Appl. Polym. Sci.* **2005**, *95*, 1073–1081.
(26) van der Beek, M. H. E.; Peters, G. W. M.; Meijer, H. E. H. *Macromolecules* **2006**, *39*, 1805–1814.
(27) Balzano, L.; Rastogi, S.; Peters, G. W. M. *Macromolecules* **2008**, *41*, 399–408.
(28) Swartjes, F. H. M. Ph.D. Thesis, Eindhoven University of Technology, The Netherlands, 2001.
(29) Bu, H.-S.; Cheng, S. Z. D.; Wunderlich, B. *Makromol. Chem., Rapid Commun.* **1988**, *9*, 75–77.
(30) Avrami, M. *J. Chem. Phys.* **1939**, *7*, 1103–1112.
(31) Avrami, M. *J. Chem. Phys.* **1940**, *8*, 212–224.
(32) Avila-Orta, C. A.; Burger, C.; Somani, R.; Yang, L.; Marom, G.; Medellin-Rodriguez, F. J.; Hsiao, B. J. *Polymer* **2005**, *46*, 8859–8871.
(33) Macosko, C. W. *Rheology, Principles, Measurements and Application*; Wiley-VCH: New York, 1994.
(34) Doi, M.; Edwards, S. F. *The Theory of Polymer Dynamics*; Clarendon Press: Oxford, 1986.
(35) Vega, J. F.; Rastogi, S.; Peters, G. W. M.; Meijer, H. E. H. *J. Rheol.* **2004**, *48*, 663–678.
(36) Somani, R. H.; Yang, L.; Zhu, L.; Hsiao, B. S. *Polymer* **2005**, *46*, 8587–8623.
(37) Acierno, S.; Palomba, B.; Winter, H. H.; Grizzuti, N. *Rheol. Acta* **2003**, *42*, 243–250.
(38) Housmans, J. W.; Peters, G. W. M.; Meijer, H. E. H. *J. Therm. Anal. Calorim.* **2009**.
(39) Boutahar, K.; Carrot, C.; Guillet, J. *Macromolecules* **1998**, *31*, 1921–1929.
(40) Boutahar, K.; Carrot, C.; Guillet, J. *J. Appl. Polym. Sci.* **1996**, *60*, 103–114.
(41) Khanna, Y. P. *Macromolecules* **1993**, *26*, 3639–3643.
(42) Gauthier, C.; Chailan, J.-F.; Chauchard, J. *Makromol. Chem.* **1992**, *193*, 1001–1009.
(43) Christensen, R. M.; Lo, K. H. *J. Mech. Phys. Solids* **1979**, *27*, 315–330.
(44) Christensen, R. M.; Lo, K. H. *J. Mech. Phys. Solids* **1986**, *34*, 639.
(45) Christensen, R. M. *J. Mech. Phys. Solids* **1990**, *38*, 379–404.
(46) Coppola, S.; Acierno, S.; Grizzuti, N.; Vlassopoulos, D. *Macromolecules* **2006**, *39*, 1507–1514.
(47) Pogodina, N. V.; Lavrenko, V. P.; Srinivas, S.; Winter, H. H. *Polymer* **2001**, *42*, 9031–9043.
(48) Hashin, Z.; Rosen, B. W. *Trans. ASME, Ser. E, 86, J. Appl. Mech.* **1964**, *31*, 223–232.
(49) Azzurri, F.; Alfonso, G. C. *Macromolecules* **2008**, *41*, 1377–1383.
(50) *De* and *Wi* are similar, but they have different physical interpretations. *De* is defined as τ/t_{exp}, with τ the characteristic relaxation time of a material and t_{exp} the observation time of the experiment, probing the response of the material. *Wi* is defined as $\dot{\gamma}\tau$ with $\dot{\gamma}$ the applied shear rate. In the context of flow-induced crystallization, *Wi* determines whether molecules are deformed sufficiently to enter the enhanced nucleation regime or to go from there to the oriented crystallization regime.[16] If $t_{exp} = t_s$, the flow time, *De* determines whether these molecules reside in that regime long enough to give rise to a noticeable change in the nucleation density or the crystalline morphology. See for example ref 17.